Chapter 17
NICMOS Error Sources

In This Chapter...

Flatfield Errors / 17-1
Dark Current Subtraction Errors / 17-7
Instrument Artifacts / 17-11
Cosmic Rays / 17-14

This chapter describes the most common sources of uncertainty affecting calibrated NICMOS data. Some of these will be propagated into the Error Array of the calibrated data (e.g., flatfield uncertainties) or into the Data Quality Array (e.g., grot and hot pixels). These sources all represent limiting factors for the sensitivity of the NICMOS observations. In addition, some error sources found during the Science Mission On-orbit Verification (SMOV) are described (e.g., non-zero zeroth read, dark current pedestal), to help observers decide whether their data need to be recalibrated or analyzed with particular care.

Many details in this chapter are based on preliminary results from the SMOV, and will evolve as our understanding of the on-orbit NICMOS performace improves. Updates will be periodically posted on the NICMOS WWW pages.

17.1 Flatfield Errors

17.1.1 Thermal-Vacuum versus On-Orbit Flatfields

A full set of flatfield frames was taken with the NICMOS arrays during the System Level Thermal Vacuum test, conducted on the ground in August 1996. However, because of the thermal short experienced by the instrument during the first month of its on-orbit life, NICMOS is operating at a slightly higher temperature than was predicted (59.5 K instead of 57 K). The response of the

detector is temperature-dependent, so some changes are expected in the on-orbit flatfields relative to the thermal vacuum results. As part of the Cycle 7 calibration program, a full set of internal and external (earth) flatfields will be obtained. Users are encouraged to recalibrate their data with on-orbit flatfields if the pipeline calibration used thermal vacuum flatfields.

Preliminary results from SMOV indicate that variations in the large scale structure of the on-orbit flatfields relative to the thermal vacuum flatfields are of the order of 1–2% in Camera 2, and up to 5% in Camera 1. Figure 17.1 shows two examples of the ratio of the on-orbit to thermal vacuum flatfields for Camera 2 and Camera 1.

Figure 17.1: Ratio of On-Orbit to Thermal Vacuum Flatfields for Camera 2 in the F110W (left) and Camera 1 in the F140W (right). The ratios are averages across 20 columns and are given as a function of row number.

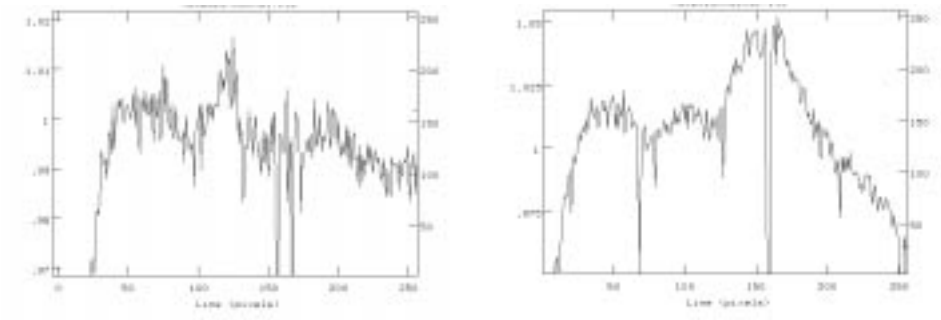

17.1.2 Characteristics and Uncertainties of Flatfields

Our current knowledge of the NICMOS flatfields is based on tests carried out using a flight spare detector array. The general characteristics are the same for the thermal vacuum flatfields, and we expect them to remain the same for on-orbit flatfields.

NICMOS flatfields show significant large-scale non-uniformity as well as pixel-to-pixel fluctuations. In addition, the non-uniformity is a strong function of the wavelength. Figure 17.3 shows the measured flatfield response for a flight spare array at a number of wavelengths. At 0.8 μm, the most sensitive areas on the array are more than twice as sensitive as the mean, and the least sensitive areas less than half as sensitive (i.e., there is variation by a factor of ~5 in the relative response across the array). This declines to a factor of ~3 at a wavelength of 2.2 μm, and at 2.5 μm the array is almost flat. We estimate that the mean uncertainties of the flat field response measurements are ~4%; the accuracy is however largely non-uniform, due to large variations in the response across the detector.

The amplitude of pixel-to-pixel variations in response is displayed in several ways in Figure 17.2, for a wavelength of 1.5 μm. The figure shows that the variations are essentially random with position on the array, and have a typical 1σ

amplitude ~8% and that the pixel-to-pixel variations are independent of the global response.

Figure 17.2: Flat Field Response Images Using 10% Bandwidth Filters on a Flight Spare Array. Wavelengths used include **(a)** 0.8μm, **(b)** 1.5μm, **(c)** 2.1μm and **(d)** 2.5μm. The images have been normalized to the mean response for each wavelength. The contours and greyscale are linearly spaced in each image between normalized responses of 0.4 and 2.2. Significant areas of the array span this whole range at 0.8μm, while at 2.5μm the array is almost flat.

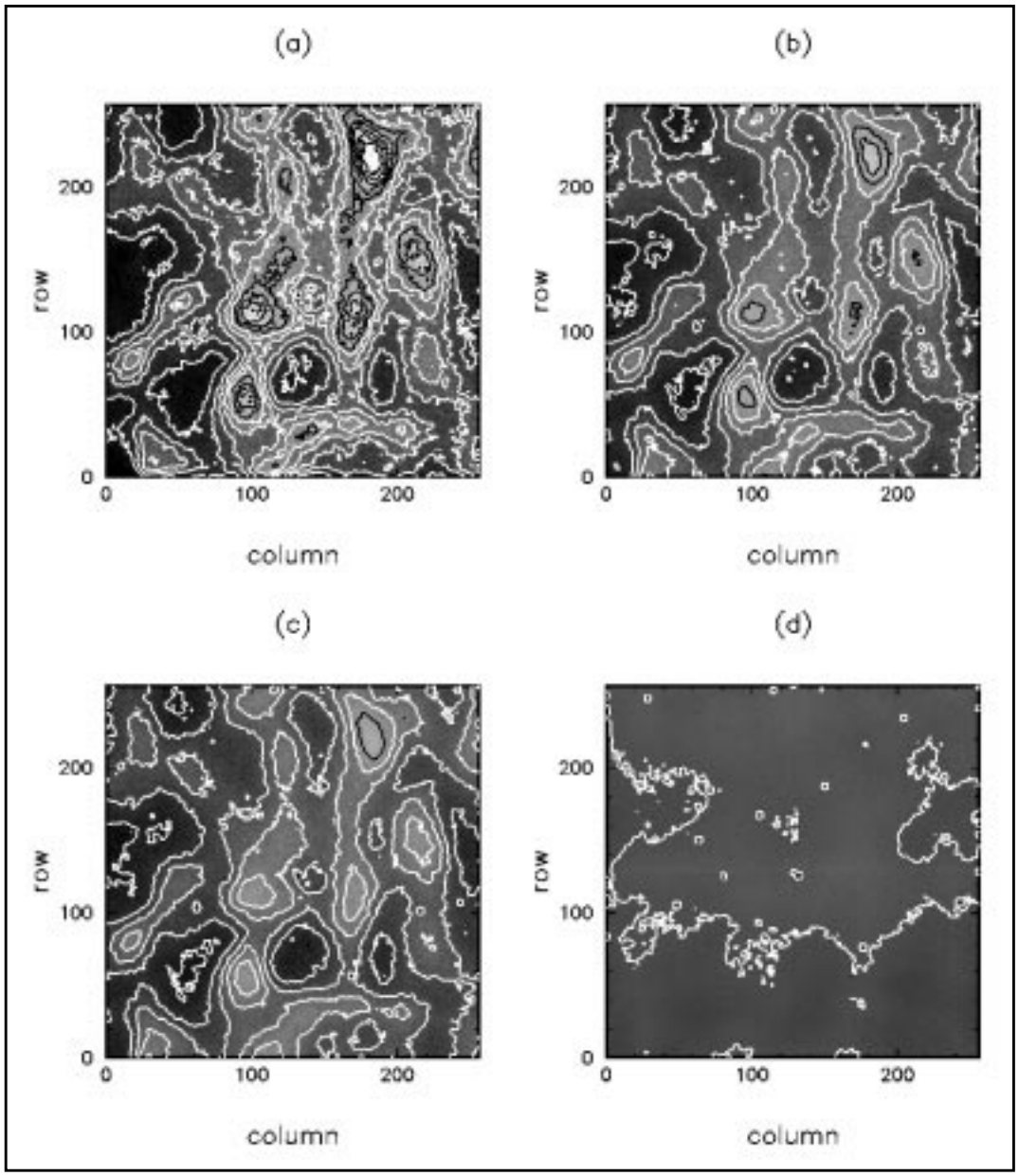

Figure 17.3: High Spatial Frequency Noise at 1.5µm. This was measured by dividing the image in Figure 17.2. (b) by a smoothed version of itself. The grey-scale version in **(a)** is scaled between 0.9 and 1.1. Slices through the image are plotted in **(b)** along row 100 and in **(c)** along column 100. The distribution of data is plotted as a histogram in **(d)**.

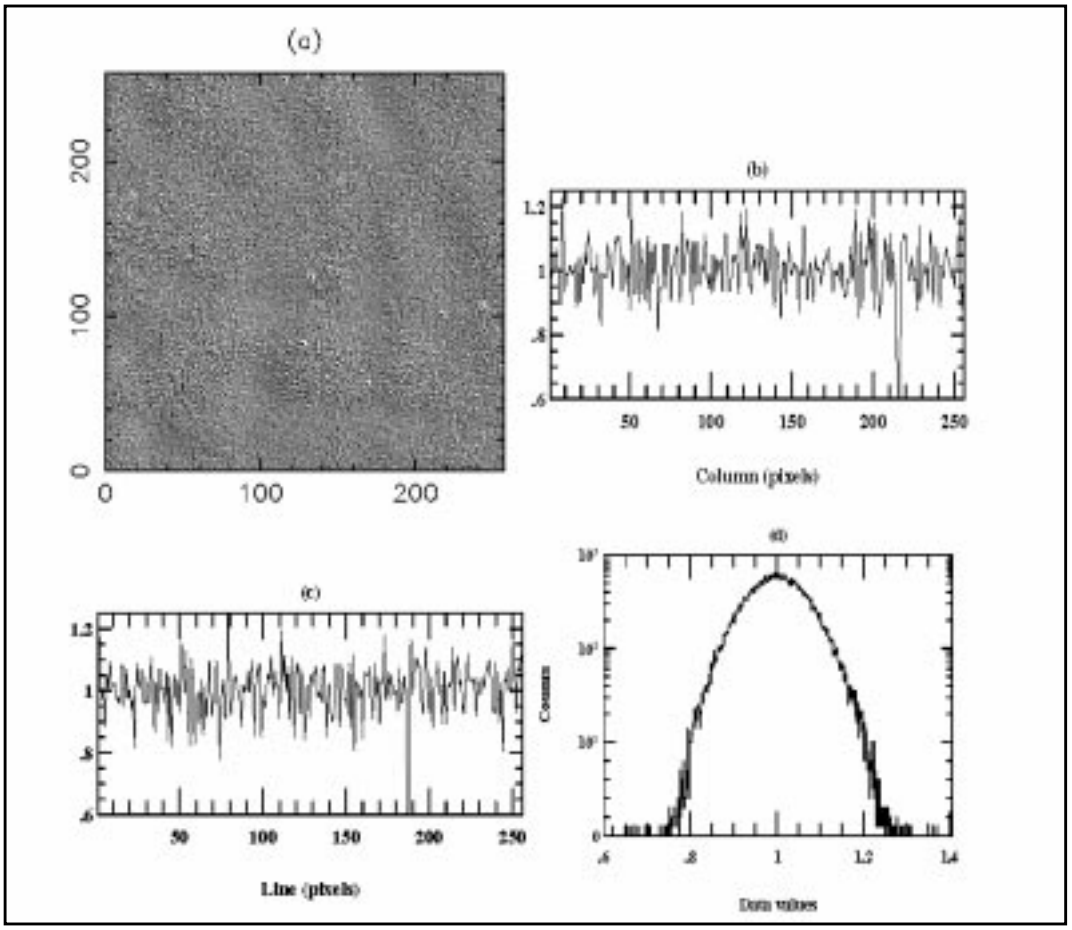

The size of the pixel-to-pixel sensitivity variations with wavelength is similar to that measured for spatial variations in the global flatfield response. At 0.8 µm the standard deviation of the pixel-to-pixel sensitivity variations is ~11%, at 1.5 µm it is ~7%, at 2.1 µm it is ~6%, and at 2.5 µm it is lower than the measurement uncertainties. Figure 17.4 shows the general behaviour of the flat-field response with wavelength, which is similar for low and high frequency variations.

The response of individual pixels relative to the mean of the array as a function of wavelength is given in Figure 17.5, for both low sensitivity and high sensitivity spots. The relative response is a slowly changing function of wavelength between 1.0 and 2.2 µm, while it changes dramatically beyond 2.25 µm, to become a linear function of wavelength.

In summary, NICMOS flatfields indicate:

- The flatfield response variations are large and wavelength dependent. The difference in response between the most and least sensitive areas is almost a factor of five at the shortest wavelengths and a factor of 1.1 at the longest wavelengths.
- The variation with wavelength is not linear, the largest variations occurring in small wavebands shortward of 1.1 microns and longward of 2.2 microns. The variations in response longward of about 2.2 microns are much more extreme than those shortward of 1.1 microns.
- The arrays exhibit wavelength dependent pixel-to-pixel response variations, ranging from an amplitude of order 10% at the shorter wavelengths to less than our measurement uncertainties at the longest wavelengths. The variation with wavelength of the pixel-to-pixel response variations is almost identical to the behavior of the global flat field response variations.

First indications from on-orbit flatfields are that all these characteristics are stable in time, and therefore calibratable with high accuracy. However, the change in temperature from the thermal vacuum experiments to the on-orbit operating conditions requires on-orbit flatfields to be used to calibrate NICMOS data.

Figure 17.4: Amplitude of Flat Field Response Variations as a Function of Wavelength. The solid line shows the global flat field response, defined as the standard deviation of the individual pixel responses, while the dashed line shows the pixel-to-pixel variations. The two follow the same behavior very closely.

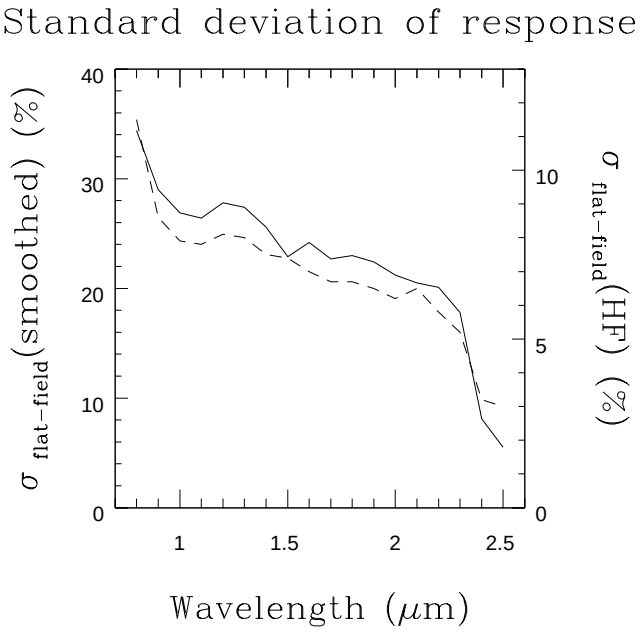

Figure 17.5: Responses of Selected Pixels Relative to the Mean of the Array as a Function of Wavelength. Both regions of low sensitivity (top panel) and high sensitivity (bottom panel) are considered. These figures show that the response flattens rapidly longward of 2.2 microns.

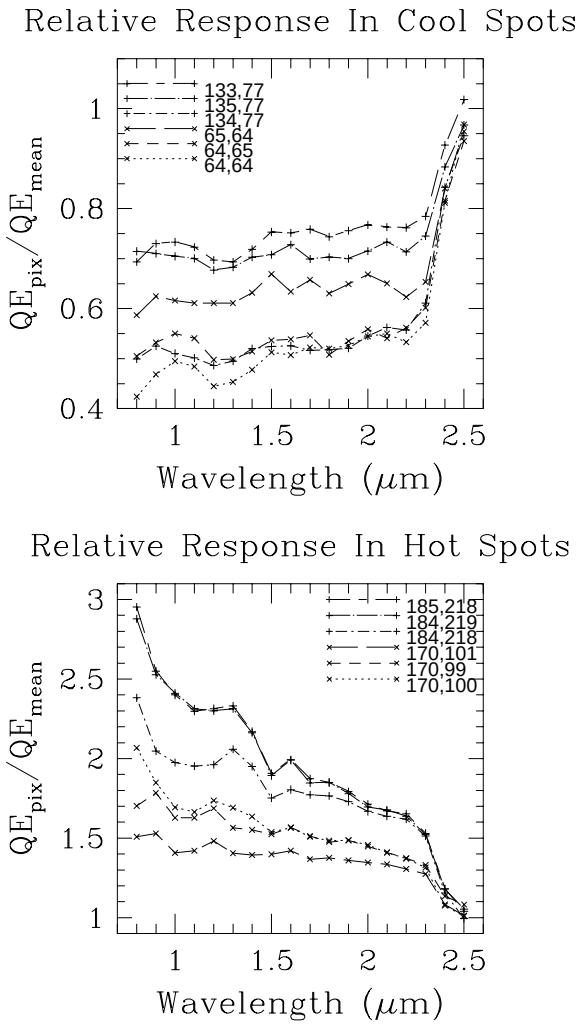

17.1.3 Color Dependence of Flatfields

The strong wavelength dependence of the NICMOS flatfields will affect the photometric accuracy of sources of extreme colors observed in broad-band filters. An estimate of the photometric accuracy which can be reached in these cases has been obtained simulating a source with color [J-K]=5 (equivalent to a blackbody with temperature T=700 K, e.g., a Young Stellar Object). The main result from the analysis is that the photometric errors are generally small: around 3% in the F110W and F140W filters, around 2% in the F205W filter, and less than 2% in the

other filters. However, they represent the limitation in photometric accuracy, unless multi-filter observations are available. In this case, an iterative correction procedure can be used to improve the photometric accuracy.

17.2 Dark Current Subtraction Errors

17.2.1 Dark Current Pedestal

NICMOS data show what is known as the *dark current pedestal*. This is an additive signal that appears whenever the detector's amplifiers are switched on, which happens at the beginning of an observing sequence, after a filter wheel motion, spacecraft motion, or Earth occultation. The level of the pedestal is quadrant-dependent and random, with typical values below 40–50 DN.

At the time of writing (August 1997) a flight software modification is being developed to remove the pedestal. The basic idea is to leave the amplifiers on at all times (instead of keeping them off, and switching them on only when exposures start). The degree to which this strategy has succeeded will not be known for some time after the change is made.

Being an additive signal, the most noticeable effect of the pedestal is to leave flatfield residuals in the calibrated images; the pedestal is a uniform offset without any flatfield variations, and so the flatfield correction step in **calnica** will impose an inverted flatfield response pattern in the final calibrated image. In addition, the absolute photometry of extended objects (i.e., those for which a reference sky level cannot be obtained within the frame) will be altered. Finally, the presence of the pedestal makes the **calnica** automatic cosmic ray rejection processing of MULTIACCUM images less effective. Since currently the pedestal effect lacks full characterization, it cannot be calibrated out by the pipeline.

For observations of compact sources, where most of the frame is occupied by blank sky, an iterative procedure can be used to remove most or all of the pedestal. The procedure exploits the large scale non-uniformity of the NICMOS flatfields, which will produce a large scale modulation of the blank sky in a calibrated NICMOS image with a considerable pedestal signal. The goal of the procedure is to remove the pedestal by minimizing the flatfield non-uniformities. This technique was thought out and developed by Mark Dickinson of the Johns Hopkins University, and is outlined below.

The procedure is iterative and identifies the minimum of the residual flatfield non-uniformities on the calibrated images (run through **calnica,** only). It should be applied on a quadrant-by-quadrant basis, becuase the pedestal level is different in different quadrants. For MULTIACCUM data, the procedure should be applied on individual imsets; however, it is not useful for the very first few readouts (where there is very little signal), and as a rule of thumb should be applied to those imsets with exposure times greater than about ten seconds. Increasing values of the pedestal level are subtracted from the each quadrant in the raw images, and the latter are run through the calibration software **calnica***, up to the flatfielding step*

only. The calibrated images are then smoothed (e.g., using the IRAF tool **rmedian**) to remove sources and pixel-to-pixel variations of the flatfield residuals. Finally, the variance of the residual large-scale modulation in each image is computed relative to the appropriate constant sky level. The pedestal level which yields the minimum for the variance is selected as the value for that particular quadrant. Because the reference value for the image is a constant sky level, it is clear why this technique can be applied only to those frames containing a large fraction of blank sky.

17.2.2 Synthetic MULTIACCUM Darks

NICMOS dark images are highly dependent on the readout history of the array since it was last reset, and, therefore, cannot be simply rescaled to the exposure time of the science data (as is done with most conventional CCD data). Each science file must be calibrated with a dark frame of equal exposure time and number of readouts.

A NICMOS dark frame can be decomposed into three basic components:

- Dark current proper.
- Amplifier glow.
- Shading (a bias change).

The three components are highly reproducible and can be easily calibrated. On-orbit darks obtained during SMOV have been used to characterize the dependence of the three components on the pixel position and on time for each of the three NICMOS detectors. This information has been used to construct synthetic dark current calibration reference files for all `MULTIACCUM` readout sequences, using as basic data the on-orbit darks obtained during the first part of the Cycle 7 calibration program. The synthetic darks have been used to populate the calibration database for those sequences for which on-orbit data do not exist yet or are currently contaminated by the dark current pedestal. These darks are routinely used to calibrate NICMOS data in the pipeline. Here we describe in more detail the three components of a synthetic dark.

Dark Current

The dark current component is the detector current when no external signal is present. This component is a function of time only:

$$D(t) = dc \times t$$

Where D is the observed signal in a given readout, t is time since reset, and dc is the dark current (e^-/s). The NICMOS dark current is of the order of 0.05–0.06 e^-/sec for Camera 2, and < 0.03 e^-/sec for Cameras 1 and 3.

Amplifier Glow

The characteristics of the amplifier glow are described in the section “Instrument Artifacts” on page 17-11. For the purpose of dark frame modelling, it is enough to know that the amplifier glow is a signal: infrared radiation emitted by

the amplifiers at the four corners of each NICMOS array, which is detected by the pixels in the array. It is like having a small light bulb in each corner, which produces a pattern of light that is highest in the corners and decreases towards the center of the array. Because the signal is injected in the array every time this is read, the amplifier glow depends on the number of readouts performed in a particular exposure. In particular, it is proportional to the number of readouts since the last reset:

$$A(x, y) = amp(x, y) \times NR$$

where *A(x,y)* is the cumulative signal due to the glow in a sequence, *amp(x,y)* is the amplifier glow signal per readout (a function of the pixel location *x,y*), and *NR* is the total number of readouts of the array since the last reset. In the corners of a full 26-readout MULTIACCUM response there will be of order 500–800 DN due to amplifier glow, as well as the associated Poisson noise from this signal. Because amplifier glow is a radiation source detected by the array, it is subject to the non-linearity and DQE characteristics of the array. The low-level non-linearity has not yet been well characterized, leaving some uncertainty in the correction. One standing problem for the characterization of the glow non-linearity is the unknown source signal in the science data images, since this is signal added to the amplifier glow signal and therefore contributes to the non-linear behavior. In many cases, the non-linearity is expected to induce small uncertainties in the final calibrated data.

Shading

Shading is a *noiseless* signal gradient, a pixel-dependent bias, orthogonal to the direction of primary clocking. The shading effectively changes the bias level for the pixels as a function of time and also of location, because the first pixels to be read show the largest bias change. Visually, this appears as a ripple and a signal gradient across a given quadrant of an uncorrected image. The amplitude of the shading can be as large as several hundred electrons for some pixels under some circumstances. The shading exhibits all the characteristics of a bias change, including lack of noise (within our measurement uncertainties). Through analysis of on-orbit dark data, we have determined that for a given pixel the bias level superimposed on the signal by the shading is dependent on the time since the last read (not reset) of the pixel. Thus if the time δt between reads remains constant, the bias level introduced by the shading remains constant. For MULTIACCUM readout sequences where the time between readouts is increasing logarithmically, the bias level changes with each successive read, and thus the overall shading pattern evolves with readout. The functional form of the shading is nearly exponential with δt and quite repeatable, although there are some circumstances when repeatability is not exact (namely, on orbit testing of the MIF sequences has shown that changing from a very long δt to a very short one introduces non-linearities in the functional form of the shading).

Although a numerical fit to the shading function is possible in principle, we have chosen to generate bias images for each of the δt of each of the

MULTIACCUM sequences from on-orbit data. In building a synthetic dark, the appropriate bias image:

$$B(x, y) = S(\delta t, x, y)$$

where *B(x,y)* is a function of the pixel location, can then be added to the other two components.

Making a Synthetic Dark

The total dark signal in *any given pixel* of any given NICMOS MULTIACCUM readout is just the sum of the three components above:

$$DARK(x, y, t) = D(t) + A(x, y) + B(x, y)$$

17.2.3 Uncertainties in the Synthetic Darks

The uncertainties in the dark frames described in this section are preliminary and will evolve as more on-orbit dark frames are obtained. Two types of uncertainties, random and systematic, can be identified in the synthetic darks.

Random Uncertainties

In the center of the NICMOS arrays, where the effects of shading and amplifier glow are smallest, the noise in the synthetic darks have uncertainties dominated by the readout noise. Because typically 15 measurements or so are used per read per pixel, the estimated uncertainities are of the order of 1 DN (about 5 electrons). In the corners of the arrays the amplifier glow is the largest source of noise, increasing as a function of the number of readouts. For the largest number of readouts (26) the estimated uncertainty is of the order of 5 DN (about 27 electrons). The random uncertainties in the dark frames are thus spatially dependent.

Systematic Uncertainties

Comparison of on-orbit to synthetic darks shows that the differences between the two are relatively small—on the order of 0 to 15 DN, with some excursions to 30–40 DN in the corners of the arrays for the final reads of full 26-readout sequences. Most of these differences are due to over- or under-subtraction of the amplifier glow. A better characterization of the amplifier glow from on-orbit data should alleviate these systematic effects.

The dark current pedestal adds some uncertainty to the synthetic darks, since on-orbit dark frames are used to generate synthetic darks. However, every effort was made to throw away pedestal-affected data when making the reference files currently in the database.

One standing problem is the proper shading correction in the second of the multiple readouts at the end of a MIF sequence. This single readout is the only one for which a shorter δt occurs after a longer one in any of the MULTIACCUM sequences. A different shading function is observed for this readout, lower by about 50–100 DN than expected for the specific δt, and with a smooth gradient

across a given quadrant in the readout direction. All previous and subsequent readouts appear unaffected by this problem. The effect of this one imperfect dark frame is typically rather small in the final calibrated image.

17.3 Instrument Artifacts

17.3.1 Non-Zero Zeroth Read Correction for Bright Sources

The first non-destructive read after a reset during a NICMOS exposure provides the reference bias level for the counts in each pixel of the science image. This is the zeroth read in a MULTIACCUM image, which is directly subtracted from the final readouts on-board the telescope for all the other readout modes so that only differences between non-destructive reads are sent back to the ground. Due to physical limitation in the readout speed, the zeroth read happens 0.203 seconds after the reset of the detector. When a bright source is being observed, a non negligible amount of charge will already have accumulated on the detector by the time the zeroth read is performed. (NICMOS doesn't have a shutter.) The consequences for the calibration of bright sources are obvious. Because the zeroth read subtraction from all subsequent readouts in a MULTIACCUM exposure is the first step of the calibration processing (and is automatically subtracted on-board the telescope from the final read in a ACCUM exposure), the handling of the detector nonlinear response will be inaccurate. At the time of this writing (August 1997) a modification of the calibration pipeline software **calnica** is being developed to correct the NICMOS observations for the non-zero zeroth read problem. The software fix requires that observations of bright sources be performed using the MULTIACCUM readout mode. The reason for this strategy is that all individual readouts are returned to the observer, and those can be used to extrapolate the counts back to the reset time (–0.203 seconds from the zeroth read) to recover the true bias level. Once the modification to the calibration pipeline software is in place, the problem will likely disappear. Then only the first few months of NICMOS on-orbit data taking will be affected (if bright sources have been observed), and those data may need recalibration.

17.3.2 Effects of Overexposure and the "Mr. Staypuft" Anomaly

Because each pixel of the NICMOS detectors is read individually, overexposure does not cause bleeding along the columns direction, unlike the case of CCDs. However, two artifacts result from the overexposure of one or more pixels:

- An afterimage with excess dark current persists for many minutes (>> 10). Decay of this signal depends both upon elapsed time and, fairly strongly, upon the number of readouts performed (ongoing modifications to the

autoflush procedure used between exposures may improve this situation). It is not unreasonable to expect signals of ~1 e^-/second up to an hour following a severe exposure.

- Extremely bright targets can result in faint phantom images at the same pixel locations in the other three quadrants of the detector. NICMOS arrays are divided into four quadrants of 128 x 128 pixels each. When a very large number of counts are recorded in a source at pixel (*i*,*j*) of any one quadrant, a faint ghost of this image appears at pixel (*i*,*j*) of each of the other three quadrants. A faint band is seen running along detector rows which pass through these ghosts, which could be mistaken for a diffraction spike. The amplitude of the ghost images is of order a tenth of a percent of the real image count rate. It appears to be an electronic phenomenon and is not an optical ghost. Inside the NICMOS group, this effect is known as the "Mr. Staypuft anomaly."

17.3.3 Vignetting

Lateral shifts of the dewar resulted in vignetting in all three cameras. In the case of NIC1 and NIC2, the source of the vignetting is most likely the Field Divider Assembly (FDA) mask. The losses in throughput are relatively small (< 5%) and affect only the first 30 rows of the arrays. In NIC3, the region affected by vignetting is larger than in the case of the other two cameras; the first 60 rows are vignetted. In this case, the source of vignetting is likely to be a combination of FDA and fore-optics. At the time of this writing (August 1997), we are evaluating the use of the Field Offset Mechanism (FOM) to move the aperture of NIC3, in order to correct at least the part of vignetting caused by the fore-optics.

17.3.4 Amplifier Glow

Each quadrant of a NICMOS detector has its own readout amplifier, which is situated close to an exterior corner of the detector. When a readout is made, the amplifier injects a real signal into the detector, known as *amplifier glow.* This signal is largest closest to the corners of the detector where the amplifiers are situated, and falls rapidly towards the center of the detector. The signal is only present during a readout, but is repeated for each readout (e.g., a MULTIACCUM sequence or an ACCUM with multiple initial and final reads). Typically the extra signal is about 20–30 DN at the corners of the detector and 2–3 DN at the center, for each readout. The signal is highly repeatable, and almost exactly linearly dependent on number of reads (however, there may be a small non-linearity for reads made very close together in time; the amplitude of this non-linearity typically amounts to only a fraction of DN accumulated over an entire `MULTIACCUM` exposure in the brightest parts of the amplifier glow signal, and our detection of this non-linearity is, at the time of this writing, marginal).

The amplifier glow is a real signal and is subject to photon statistics, so it is a source of noise in NICMOS exposures. Thanks to the repeatibility of the signal, images calibrated with the appropriate dark frames (same MULTIACCUM

sequence or same exposure time for ACCUM images) will have the amplifier glow removed. Its noise is propagated into the ERR array of the NICMOS calibrated images, thanks to its Poissonian nature.

17.3.5 Intra-Pixel Sensitivity Variations

As with many other modern array detectors, the sensitivity of the NICMOS detectors is lower near the edges of pixels then in their centers, causing reduced sensitivity along the intra-pixel boundaries. The response of a pixel to a source whose flux changes rapidly on a size scale comparable with or smaller than the pixel size will thus depend on where the center of the source lies with respect to the center of the pixel. Because the latter is not known a priori, this effect will introduce some uncertainty in the flux calibration for a point source. This uncertainty will be largest for Camera 3 at short wavelengths, for which the PSF is undersampled. We will try to measure the size of this effect on orbit and post updates on the NICMOS WWW pages; we expect it to be no more than a few percent uncertainty for Camera 3.

17.3.6 Hot Pixels, Cold Pixels, and Grot

The statistics on the cold and hot pixels present in each of the NICMOS cameras are presented in Table 17.1 below. In NIC2, the presence of the coronographic spot increases the number of cold pixels to 154.

In addition to these bad pixels which were already known from ground-based testing, more pixels have shown low measured quantum efficiency in orbit. These pixels are possibly affected by debris lying on top of the detectors. Paint flakes from the optical baffles are one possible source. Currently about 150–200 of these bad pixels have been measured in NIC1 and NIC2, and similar numbers are expected for NIC3. The bad pixels are often clustered in groups of up to 20–40, and appear as dark spots in flatfield frames. The position of the flakes varies.

Table 17.1: Statistics on Cold and Hot Pixels and Grot

Pixel Characteristic	NIC1	NIC2	NIC3
COLD	68	94	17
HOT	10	11	3
GROT	~ 200	~ 150	...

17.4 Cosmic Rays

As with CCDs, cosmic ray hits will produce unwanted signal in the output images, but hot pixels are not expected to develop from such hits. Hence, cosmic rays should have little impact on the long-term array performance in orbit.

Analysis of SMOV data has shown that the rate of cosmic rays on the NICMOS detectors is about 1.2–1.6 events/Camera/sec (5 σ detections, see *Instrument Science Report* NIMOS-022). The mean size of the cosmic ray (CR) hits is 1.65 to 2 pixels. Table 17.2 below summarizes cosmic ray statistics for the three cameras, for 5 σ and 3 σ detections. The numbers for Camera 2 come from two different programs and indicate variations of about 60% in the rate of CR-affected pixels between the two observations; the variations reflect changes in the orbital position of the telescope relative to the South Atlantic Anomaly. This level of variation is what should be expected during a typical multi-orbit program.

Table 17.2: CR Event Statistics

Camera	Threshold	Affected Pixels (#/Camera/sec)
NIC1	5 σ	2.11
NIC1	3 σ	2.74
NIC2	5 σ	1.99-3.21
NIC2	3 σ	2.43-3.96
NIC3	5 σ	1.90
NIC3	3 σ	2.79

For a mean CR-affected pixel rate of about 2.5 pixels/sec, about 8% of the pixels in the detector will show cosmic ray events in a 2000 second exposure.

CR hits should be detected by **calnica** in MULTIACCUM data, and will be flagged in the DQ extensions of the `*_ima.fits` files.

17.5 Calibration Goals

The Cycle 7 calibration goals for NICMOS are listed in Table 17.1 below. Since NICMOS is expected to run out of cryogens between the end of 1998 and the beginning of 1999, these represent the final calibration goals for the instrument. The main limiting factor for attaining such goals will be the thermal stability of the instrument. The Table summarizes the accuracy we expect to

achieve for reference files, photometry, astrometry, etc. (cf. the NICMOS Instrument Manual).

Table 17.1: NICMOS Calibration Goals

Attribute	Accuracy	Comments/Limiting Factors
MULTIACCUM and ACCUM darks	10 ADU	All three detectors. All the supported MULTIACCUM sequences and a subset of ACCUM exposure times will be calibrated to this accuracy. Other ACCUM exposure times will require interpolation.
Flatfields	2% global uncertainty <1% pixel-to-pixel	NIC1 and NIC2 (reduced program for NIC3). Flatfields will be obtained from a combination of internal lamp flats (1% accuracy, polarizers, broad and medium band filters) and Earth flats (2% acccuracy, narrow band filters). Color dependence may limit flatfields in some cases.
Photometry	5-10% absolute 2% relative over field-of-view 2% stability	Main limiting factors: accuracy of standards; filter leaks on red sources
Focus position	maintained within 1 mm	Instrument focus will be monitored throughout the entire Cycle 7 in all three cameras
Polarizers	1% relative photometry 3–5% absolute polarization	Instrumental polarization and zero position angle of NIC1 and NIC2 will be measured. Limiting factors: dark and flatfield uncertainties; polarizing efficiency.
Grisms	0.01 μm (wavelength calibration) 20%-30% (absolute and relative photometric sensitivity)	Expected accuracy over central 80% of spectral range. Grism C flat may not achieve the declared accuracy.
Coronagraph	0.019" positioning	Hole and detector are not at common focus
NICMOS to FGS astrometry	0.1"	
Plate Scale Calibration	0.2%	